ELSEVIER

Applied Surface Science 180 (2001) 227–245

applied surface science

www.elsevier.com/locate/apsusc

Physico-chemical behavior of carbon materials under high temperature and ion irradiation

T. Paulmier[a], M. Balat-Pichelin[a,*], D. Le Quéau[b], R. Berjoan[a], J.F. Robert[a]

[a]*Institut de Science et de Génie des Matériaux et Procédés, IMP-CNRS, BP 5, 66125 Font-Romeu Odeillo, France*
[b]*Centre d'Etude Spatiale des Rayonnements, CESR-CNRS, 9 av. du Colonel Roche, 31029 Toulouse, France*

Received 6 June 2000; accepted 14 May 2001

Abstract

Carbon/carbon (C/C) composites have been chosen for the conception of the thermal shield of the ''Solar Probe'' space mission. To understand their behavior under solar aggressions (high temperature and ion irradiation) and know the possible interactions with the shipped-in instruments, these materials are tested in a facility that allows to partially simulate the solar environment and to carry out in situ measurements. The mass loss rate of the materials is recorded and the composition and distribution of the ejected species are followed using an opened source mass spectrometer and a post-treatment XPS analysis of the condensed species on a gold-plated copper target is also performed. Besides this, the sputtering processes of graphite at high temperature and ion irradiation have been theoretically investigated in order to understand the main parameters that can influence the erosion of the material and predict accurately the physico-chemical behavior of the C/C composites.

Keywords: Carbon composites; Sun; High temperature; Ion irradiation; Modeling

1. Introduction

A space mission ''Solar Probe'' is currently in progress for the exploration of the solar winds and the solar corona at 4 solar radii from the Sun by in situ measurements.

The spacecraft will be affected by the close range to the Sun and needs thus to be shielded from the intense solar flux, allowing to the various instruments working at ambient temperature. To prevent interference with scientific measurements, the mass loss rate from the shield surface should not exceed 5.8×10^{-4} g m^{-2} s^{-1} for temperature above 2200 K.

Several materials satisfy this requirement but carbon–carbon composites seem to be the most interesting due to their high melting point, their low density and good strength-to-weight ratios [1,2]. These materials have good thermo-radiative properties with high values and a stable ratio of solar absorptivity to total hemispherical emissivity, so that the temperature of the shield stays in adequate level due to its efficient rejection of solar heat loads. Moreover, it can be easy to modify their physical properties through the processing techniques and their structures.

It is important to determine the composition and distribution of the outgassing species and to measure the mass loss rate of the material at high temperature and under proton irradiation in order to determine the ''secondary atmosphere'' emanating from the shield. The high temperatures and the proton irradiation can

* Corresponding author. Tel.: +33-468-307768; fax: +33-468-302940.
E-mail address: balat@imp.enrs.fr (M. Balat-Pichelin).

0169-4332/01/$ – see front matter
PII: S0169-4332(01)00351-8

alter the surface radiative properties and we need then to understand accurately the physico-chemical sputtering processes of carbon–carbon under these various conditions.

The energy of hydrogen ions hitting the shield at perihelion (taking into account the speed of the probe) is about 2 keV with a flux of 5×10^{16} ions m^{-2} s^{-1}. The materials will be tested at high temperature, between 1800 and 2400 K, which are the temperatures of the shield along its surface at perihelion.

Only few experiments on carbon materials irradiated by H^+ ions have been done for temperature above 1800 K and this study allows to understand the physico-chemical erosion processes at this temperature level.

2. Fundamental processes on proton–carbon interaction at high temperature and modeling

The interaction of energetic hydrogen ions with graphite and carbon compounds and the induced dominant mechanism of erosion have been hugely studied for the use of these materials as plasma facing wall in the fusion devices Tokamak [3–22]. These interactions lead to several physico-chemical processes that can result in a high sputtering yield and to hydrocarbons and carbon atoms emission and give to graphite a special behavior, compared to metals. In fact, contrary to the metals for which the sputtering yield does not depend on target temperature, the graphite shows a steady increase of the yield above 1500 K.

When graphite is irradiated by hydrogen ions, at high temperature, it may be sputtered due to three processes:

- the physical sputtering, which implies collisional processes and is characterized by C_1 emission [3–8];
- the chemical sputtering, which is due to a chemical affinity between the implanted particles and the target material and come to molecules formation [4,7–10];
- the thermal sublimation and the radiation enhanced sublimation (RES): the thermal sublimation dominates for temperature above 2000 K and consists essentially of the emission of C_1, C_2 and C_3 clusters. The RES is peculiar to graphite and carbon materials and is characterized by only mono-atomic carbon emission [7,8,12–15].

2.1. The physical sputtering

The physical sputtering occurs for all materials, independently of the chemical nature of the projectile and target atoms and of the temperature. It results from a nuclear energy transfer of the projectile to the target atoms, leading to atomic displacements, thus causing lattice damages and sputtering. The surface atoms are ejected if they have received a sufficient kinetic energy to overcome the surface binding energy E_s of the solid.

The interaction of energetic particles, the collisional and physical processes, especially the physical interaction of graphite with H^+ ions, have been well developed in the last 30 years by numerous authors [3–22].

The physical sputtering yield at normal incidence can be described by the Bohdansky formula [7,22] which gives a good agreement with experimental data in the keV region

$$Y(E_0) = QS_n(E_0)\left[1 - \left(\frac{E_{th}}{E_0}\right)^{2/3}\right]\left[1 - \frac{E_{th}}{E_0}\right]^2 \quad (1)$$

where E_0 is the incident energy, E_{th} the threshold energy, i.e. the minimum energy to have a sputtering yield, and Q a fitting parameter. $S_n(E_0)$ is the nuclear stopping power, which can be approximated by the relation based on the Thomas–Fermi potential.

A non-perpendicular angle of incidence enhances the sputtering yield. Its angular dependence is well described by the Yamamura formula [7,22]

$$Y(\theta) = Y(\theta = 0)(\cos\theta)^{-f} \exp[f(1 - \cos\theta^{-1})\cos\theta_{opt}] \quad (2)$$

where θ is the angle of incidence, f and θ_{opt} are used as fitting parameters. The different parameters for proton incident on carbon foils are given in [21,22]. Figs. 1 and 2 give the incident energy and angular dependencies of the sputtering yield obtained by Eqs. (1) and (2).

Using our experimental conditions (H^+ with a flux of 5×10^{16} ions m^{-2} s^{-1}, an energy and angle of incidence respectively equal to 2 keV and 45°), we get for the physical sputtering of graphite due to H^+

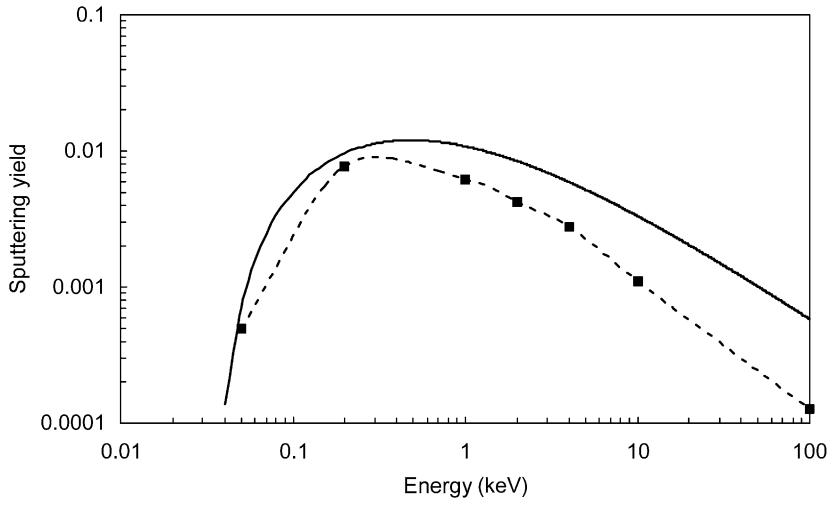

Fig. 1. Dependence of the sputtering yield of graphite on incident energy for hydrogen ions at normal incidence, calculated with TRIDYN (points and dotted line) and with the Bohdansky formula (continuous line).

impact a value of 1.8% which corresponds to a monoatomic carbon flux of 9.1×10^{14} atoms m^{-2} s^{-1}.

We have also studied theoretically the physical sputtering of graphite by H^+ ions using the TRIDYN code that has been developed by Möller et al. [6]. This program is a dynamic version of the TRIM code [23] and takes into account the composition changes in real time due to the deposition of the projectiles and the collisional transport. It can thus simulate the fluence dependent phenomena like sputtering and reflection, and allows to obtain accurate results in good agreement with experimental data.

Both these codes are based on the binary collision approximation, assuming that the target is amorphous. They are well described in [5,6]. The Kr–C potential is taken as interaction potential, the local and non-local inelastic energy losses are simulated respectively by the Lindhard–Scharff [24] and Oen–Robinson models [3,5]. The input data related to graphite for physical sputtering calculations with TRIDYN are given in [6].

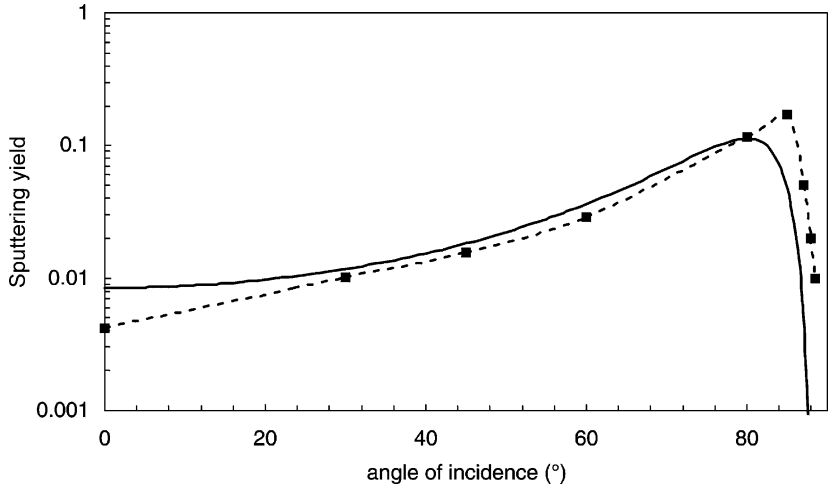

Fig. 2. Dependence of the sputtering yield of graphite on the angle of incidence for hydrogen ions (2 keV) calculated with TRIDYN (points and dotted line) and with the Yamamura formula (continuous line).

The aim of this study, in relation to the previously empirical formula (1), is to understand theoretically the damage induced by the incident ions in the bulk of graphite. With this code, we can study the distribution of hydrogen atoms within the depth, the distribution of Frenkel pairs, the penetration length in the material.

The ionized species emitted by the material are especially due to the backscattering of the incident ions at the surface of the material. It is therefore interesting to study theoretically the backscattering of the incident ions and their penetration depth using the TRIDYN code.

We have studied the energy and angular distributions of the backscattered ions and carbon atoms in our conditions. The emission of the backscattered ions is nearly isotropic from 2 to 1830 eV with a maximum at around 2 eV. The hydrogen particles will be mainly ejected with a 46° angle in good agreement with the angle of incidence. The mean energy of the reflected ions is around 400 eV, which corresponds to a mean energy loss of 80%. The energetic and spatial distributions of the sputtered carbon atoms spread from 7 to 550 eV with a mean value equal to 36 eV and a maximum around 9 eV, and from 0 to 80° for the polar angle with a mean value of 25° and a maximum in distribution at 2°. The maximum penetration depth of the incident ions is equal to 50 nm, which means that the ions have no effect on the microstructure damages beyond 50 nm. The maximum depth for the formation of Frenkel pairs is, in our conditions, equal to 75 nm. Thus, the damages induced by ion irradiation are located between the surface and 75 nm in depth, and that above this value, only the high temperatures will be responsible of damages and modifications of the microstructure of the material.

In Figs. 1 and 2, the sputtering yield obtained with the code TRIDYN presents a maximum around 200 eV (Fig. 1) in energy and 85° (Fig. 2) for the angle of incidence. The sputtering yield obtained in our experimental conditions is 1.5% in good agreement with the result obtained using the Bohdansky formula (1.8%).

2.2. The chemical sputtering

The chemical reactions between hydrogen ions and graphite are complex and lead to the emission of hydrocarbons [4,7,8,10,11,20,21]. We actually have a good overview of the main chemical mechanisms for temperature under 1000 K.

After a collision sequence, the ions penetrate at a depth of about a few hundred nanometers and are implanted in the graphite, diffuse in the bulk material and get trapped. Finally, the hydrogen will react with carbon atoms or recombine with implanted hydrogen atoms at the end of their range. These reactions lead to the emission of hydrocarbons (such as CH_4, C_2H_x, CH_3 radicals and heavier hydrocarbons) and H_2 molecules.

The theoretical studies of Balooch and Olander [11] led first to a reaction model for irradiation of carbon by hydrogen atoms and can be applied for hydrogen ions with a weak energy (since this reaction occurs near the surface). This model can explain the formation of methane, acetylene and H_2 (Fig. 3).

According to this model, and without taking into account the molecular diffusion, the acetylene and H_2 are the main reaction above 1000 K and the formation yield can be written as

$$Y_{C_2H_2} = \frac{1}{\phi_H}(K_2^2 K_6 C_H^2) \tag{3}$$

$$Y_{H_2} = \frac{1}{\phi_H} K_1 C_H^2 \tag{4}$$

with ϕ_H the incident fluence of hydrogen ions and C_H, the hydrogen topmost layer concentration.

Wittmann and Küppers [20] and Roth [21] have explained the chemical erosion and the hydrogenation at the surface of carbon materials according to an atomistic process: their models deal with a change of the hybridization (from sp^2 to sp^3) due to incident H atoms. The methyl radical is the eroding agent.

In the case of energetic hydrogen ions (instead of hydrogen atoms), the process is slightly different since the energetic ion impact comes to lattice damages, dangling bonds or interstitial formations reacting more easily with hydrogen atoms. Moreover, a kinetic emission of hydrocarbons due to collisional processes is added to the thermal emission. Roth's model [10] takes into account both thermal and kinetic emissions in order to calculate the chemical sputtering yield. In this model, as for the model of Balooch and Olander [11], at temperatures above 700 K, the H-atoms implanted in carbon materials recombine as H_2 molecules.

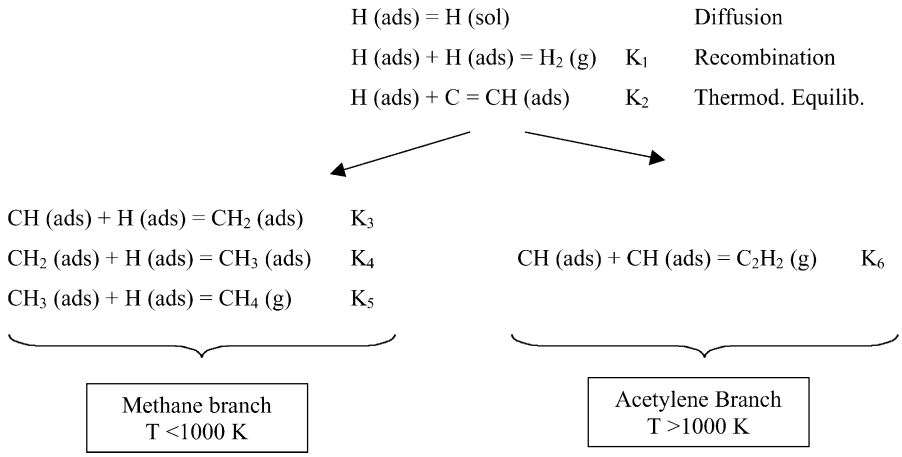

Fig. 3. Chemical reactions of graphite with atomic hydrogen (from [11]).

For the moment, the emission of hydrocarbons heavier than acetylene is not clearly understood and a calculation of their theoretical flux using the previously described model would be more or less inaccurate. The fluxes of acetylene and H_2 have been calculated using the Balooch model. The sputtering yield corresponding to the emission of methane has been calculated in our conditions using the Roth's model, assuming that the methyl radical is hydrogenated during the thermal diffusion in the material.

One gets the temperature dependence of the methane, acetylene and H_2 fluxes (Fig. 4). So, we can see that, in our conditions, acetylene and H_2 are the main emitted species and the acetylene flux is respectively equal to 8.9×10^{14} molecules $m^{-2}\,s^{-1}$ at 1800 K and 5.8×10^{15} molecules $m^{-2}\,s^{-1}$ at 2400 K. Thus, this flux is expected to be of the same order as the flux of mono-atomic carbon due to physical sputtering (9.1×10^{14} atoms $m^{-2}\,s^{-1}$). No methane is expected.

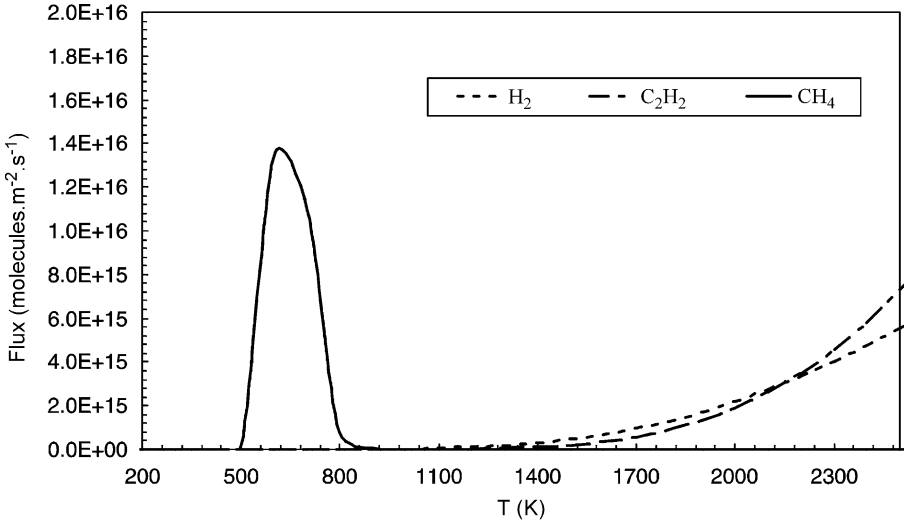

Fig. 4. Calculated H_2, methane and acetylene fluxes emitted by graphite irradiated by hydrogen ions (2 keV, 5×10^{16} $m^{-2}\,s^{-1}$) versus temperature using Roth and Garcia-Rosales [10] and Balooch and Olander [11] models.

2.3. Sublimation of graphite

In our temperature range and in the high vacuum of the chamber, graphite will loose mass by sublimation. We can thus assume that the effects of recondensation on the surface are unimportant and that the equilibrium vapor pressure for each carbon species is equal to their partial pressure. The rate of vaporization for each carbon species i is given by the Langmuir–Knudsen equation. The total rate of vaporization thus writes

$$\dot{m}_i(T) = \sum_{i=1}^{n} \alpha_i P_i(T) \left(\frac{M_i}{2\pi RT} \right)^{1/2} \quad (5)$$

where $\dot{m}_i$ is the mass loss rate (g m^{-2} s^{-1}) of species i, α_i the vaporization coefficient, P_i the equilibrium vapor pressure, M_i the molecular weight, T the temperature, and R the universal gas constant.

Using the thermodynamic data given in JANAF tables [25] for the equilibrium vapor pressure of the various carbon species and the commonly used vaporization coefficients ($\alpha_1 = 0.24, \alpha_2 = 0.50, \alpha_3 = 0.023, \alpha_4 = 0.25, \alpha_5 = 0.0019$), Eq. (5) allows us to calculate the mass loss rates for each the carbon species C_1 through C_5 and the total mass loss rate as a function of temperature. The results are plotted in Fig. 5. In the temperature range from 1800 to 2400 K, the most important species are C_1, C_2 and C_3. The mass loss rates and so the carbon species flux increase drastically with temperature, by a factor of 10 for each 100 K step. This steep increase thus requires to control very accurately the temperature of the material.

The total mass loss due to sublimation obtained by adding the mass loss of each species i leads for a mean temperature value of the thermal shield of 2100 K to 2.8×10^{-6} g m^{-2} s^{-1}, that is under the required specification of the Jet Propulsion Laboratory (JPL, NASA) of 5.8×10^{-4} g m^{-2} s^{-1}.

2.4. The RES

For temperatures above 1500 K, the erosion of graphite is dominated by sublimation and by an erosion process peculiar to graphite called RES [12–15]. This last effect has only been observed for graphite and is characterized by a steady increase of the sputtering yield with temperature. The RES is not a chemical process since it occurs for hydrogen as well as for inert ions like He or Ar. The sputtering yield due to the RES does not depend on the chemical nature of the incident ions and can exceed by a factor of 10 the

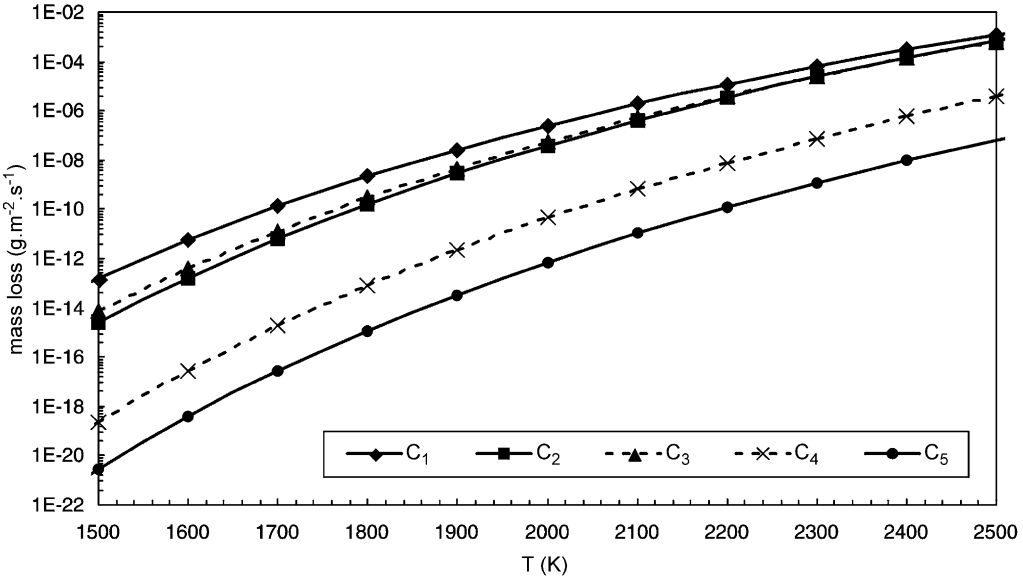

Fig. 5. Calculated mass loss rate (g m^{-2} s^{-1}) of the different carbon species C_1 to C_5 due to graphite sublimation versus temperature.

physical sputtering yield. The temperature dependence of this sputtering yield Y_{RES} is exponential

$$Y_{RES} = Y_0 \exp\left(-\frac{E_{RES}}{k_B T}\right) \quad (6)$$

where E_{RES} is the activation energy which varies between 0.75 and 0.85 eV, for hydrogen as well as for argon, k_B the Boltzmann constant, and Y_0 an experimental factor. E_{RES} remains stable for fluxes located between 10^{17} and 10^{19} ions $m^{-2}\,s^{-1}$ and increases slightly with stronger flux (10^{22} ions $m^{-2}\,s^{-1}$). With high incident energy, E_{RES} decreases to reach values of about 0.55 eV. The average value which was chosen, by supposing, like for the physical sputtering that E_{RES} does not depend on temperature is 0.78 eV [14].

The RES process consists of the emission of mono-atomic carbon with thermal energies and an isotropic angular distribution. This process can be explained using a collisional model: when incident ions collide the carbon atoms, part of their energy is transferred to the atoms of the network which are dislodged out of their lattice site towards an interstitial position. The interstitial atoms have a large mobility throughout the basal plane and diffuse towards the surface. They can also recombine with vacant sites or agglomerate to form clusters. The interstitial atoms that reached the surface are slightly related to this surface by a Van der Waals force and escape thermically very easily from the material.

The model proposed by Roth and Möller [13] and next by Philipps et al. [14] describes quantitatively the radiation enhanced erosion of graphite under ion bombardment at elevated temperatures in good agreement with experimental results. This model takes into account the creation of interstitial carbon atoms in the graphite due to nuclear collisions, the diffusion processes responsible for the migration of the interstitial atoms at the surface and of the recombination and annihilation of interstitial atoms and vacancies.

Supposing a homogeneous defect production within the diffusional range of interstitial atoms and vacancies and taking a zero concentration at the surface for both defects, the RES yield in steady state may be written as [13,14]

$$Y_{RES} = \frac{2}{\sqrt{3}}\left(\frac{D_i D_v}{K_{i,v}\Omega\phi X_0^3}\right)^{1/4} \quad (7)$$

where ϕ is the flux of incident ions, X_0 the depth in which one Frenkel pair per incident ion is produced, D_i, D_v and $K_{i,v}$ respectively the diffusion coefficients and recombination rates for interstitial atoms and vacancies, and Ω the atomic volume. The number of interstitial atoms produced per ion, the defect production distribution and the average penetration depth of ions can be calculated with a collisional process model like TRIM [5,23]. According to Eq. (7) and using the TRIM code to obtain the distribution of produced defects, we can draw the temperature dependence of this sputtering process. The different factors used in Eq. (7) are obtained by fitting the experimental results [14]. The TRIM results give us a production rate of Frenkel pairs equal to 2.1 per incident ion. We can therefore draw the carbon flux emitted due to the RES process by carbon under H^+ irradiation with 2 keV energy and an incident flux of 5×10^{16} ions $m^{-2}\,s^{-1}$, assuming that the angle of incidence has a weak effect on the sputtering yield (Fig. 6). From this calculation, the sputtering yield due to RES is expected to be equal to 4.7×10^{15} atoms $m^{-2}\,s^{-1}$ at 1800 K and to 1.9×10^{16} atoms $m^{-2}\,s^{-1}$ at 2400 K and it is around 5 to 20 times greater than the physical sputtering yield in our experimental conditions.

2.5. Summary of the sputtering processes of graphite at high temperature

From these calculations, we can draw the sputtering of graphite irradiated by H^+ ions with 2 keV energy and an incidence angle equal to 45° according to temperature and know what are the main sputtering processes and erosion level (Fig. 7). Tables 1 and 2 summarize the dominant processes in the different temperature ranges. Between 1800 and 2400 K, two processes dominate the sputtering: the RES overcomes the thermal sublimation below 2000 K. Above this temperature, the steep increase of the sputtering yield is especially due to the thermal sublimation of graphite. The released particles are thus mainly mono-atomic carbon up to 2000 K, whereas the thermally sublimed species exceed the radiation induced C_1 atoms above this temperature. The energy distribution is thus quite different from one temperature range to the other.

These theoretical results will then be compared to our experimental ones for a better understanding of the main sputtering processes of the C/C composites.

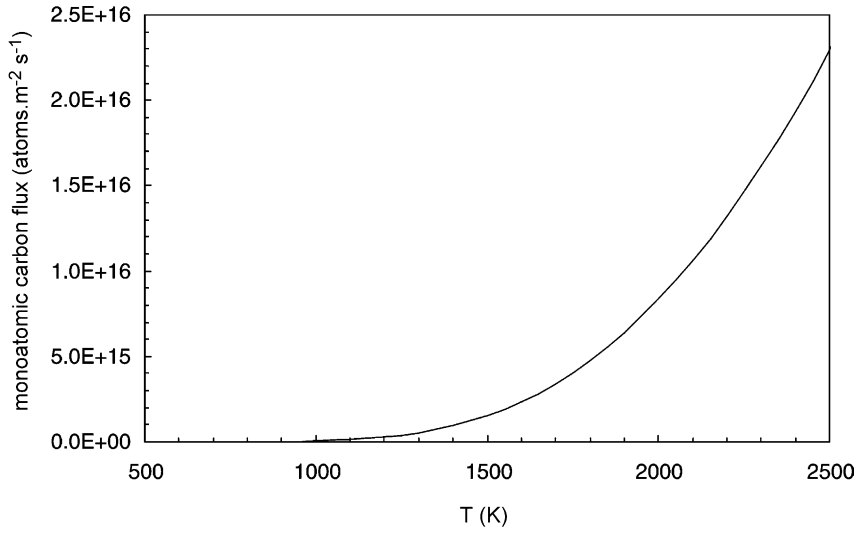

Fig. 6. Temperature dependence of the RES sputtering yield (mono-atomic carbon flux) calculated with the model in our conditions (H^+, 2 keV, 5×10^{16} ions m^{-2} s^{-1}, 45°).

3. The experimental device MEDIASE

A test facility called MEDIASE (for Moyen d'Essai et de DIagnostic en Ambiance Solaire Extrême) has been designed and instrumented in order to simulate the solar environment and characterize the carbon–carbon composites by measuring their thermo-radiative properties, their mass loss rate and analyze qualitatively and quantitatively the neutral and ionized ejected vapor species.

This test facility (Fig. 8) is placed at the focus of the 1000 kW solar furnace in Odeillo, France. The

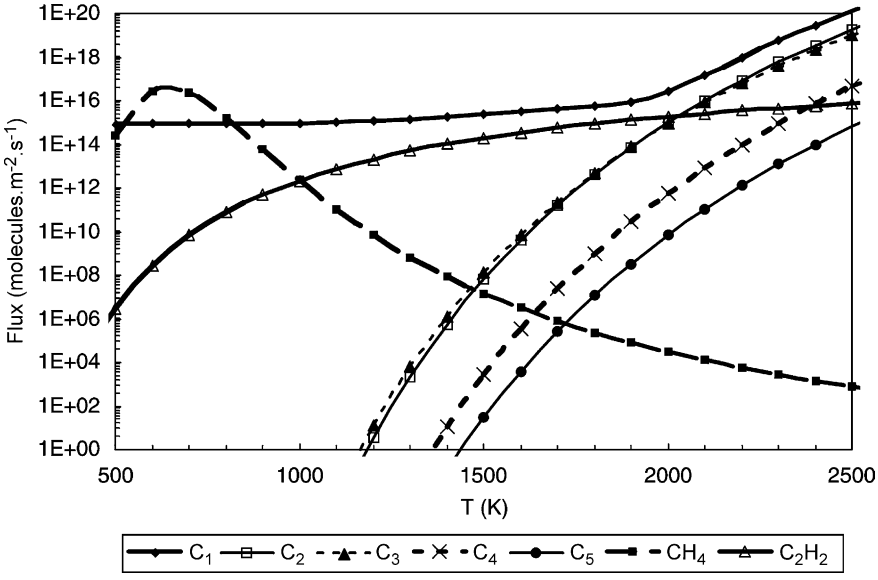

Fig. 7. Evolution of the calculated flux (molecules m^{-2} s^{-1}) of the different emitted carbon species in the temperature range, under ion irradiation (H^+, 2 keV, 5×10^{16} ions m^{-2} s^{-1}, 45°).

Table 1
Theoretical total mono-atomic carbon flux (atoms $m^2 s^{-1}$) according to the temperature and the different sputtering processes

	1800 K	2100 K	2400 K
Physical sputtering	9.1×10^{14}	9.1×10^{14}	9.1×10^{14}
Chemical sputtering	1.8×10^{15}	5.2×10^{15}	1.2×10^{16}
RES	4.7×10^{15}	1.1×10^{16}	1.9×10^{16}
Thermal sublimation	1.3×10^{14}	1.4×10^{17}	2.9×10^{19}

Table 2
Theoretical main sputtering processes of graphite under H^+ irradiation depending on the temperature range

Temperature range (K)	Main sputtering process
0–500 and 900–1300	Physical sputtering
500–900	Chemical sputtering
1100–2000	RES
2000 and more	Thermal sublimation

advantage of such a heating mode is that very high temperatures can be reached in a few seconds. The materials are heated up to 2500 K by concentrated solar radiation under high vacuum. The set-up is composed of a chamber with a capacity of around 6×10^{-2} m^3 equipped with turbomolecular and roots pumps which permits to reach a pressure of about 10^{-7} hPa. During the tests, the residual pressure rises up to 5×10^{-5} hPa. An hemispherical silica–glass window, 35 cm in diameter, is placed in front of this chamber and allows to irradiate in high vacuum the front face of the sample with the concentrated solar radiation. The sample, 40 mm in diameter and 2–3 mm thick, is maintained by a water-cooled holder with three metallic needles to minimize the heat losses to the holder. The front face of the chamber receiving the concentrated solar flux is also water-cooled.

On the back face of the sample, temperature, mass loss and optical measurements can be performed due to a water-cooled measuring chamber keeping free the instruments from parasitic radiation of the surroundings. Finally, several tubes have been implemented around the chamber to insert the ion and UV sources, and the measuring instruments.

The samples are irradiated by H^+ ions with an ion source (Fisons EX05). The current density (0.8 μA cm^{-2}) chosen for our experimental conditions corresponds to an ion flux of 5×10^{16} ions $m^{-2} s^{-1}$ with an energy of 2 keV. This ion gun is commonly used as an etching source in Auger, XPS or in SIMS analyses. In our test facility, it is located at 40 cm distance from the sample and irradiates it with a 45° angle of incidence. The beam on the target is 15 mm in diameter. The fluence and the size of the beam at the target are determined with a Faraday plate collector which can be placed between the ion gun and the target to adjust the gun parameters.

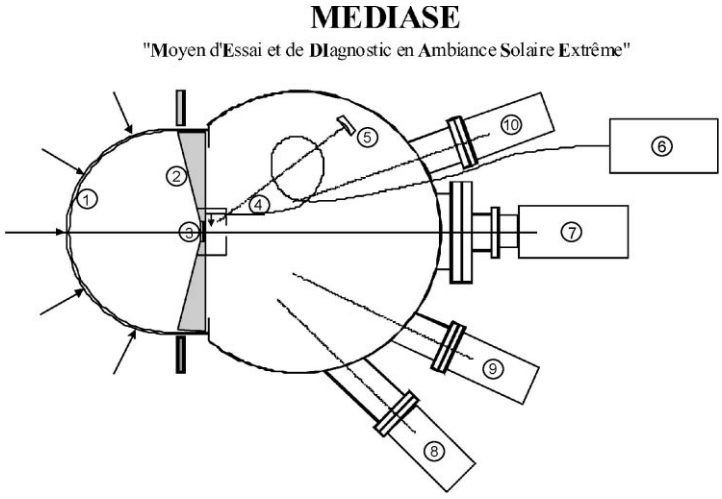

Fig. 8. MEDIASE experimental set-up: (1) hemispherical quartz window, (2) water-cooled holder, (3) sample, (4) optical fiber, (5) quartz microbalance, (6) bi-chromatic optical pyrometer, (7) mass spectrometer, (8) and (9) ion source, (10) UV source.

The test facility allows to perform several measurements when the sample is heated and irradiated. Temperature is measured with an original optical-fiber bi-chromatic pyrometer, especially designed in our laboratory for in situ measurements in severe conditions.

A quartz microbalance (Leybold-Inficon IC/5) allows to record the mass loss rate of the samples. This instrument is based on the sensitivity of the resonance frequency of a monitored quartz crystal to added mass and it is easy to return from the deposit thickness to the mass increase. The resolution is 5×10^{-4} to 10^{-3} nm for the thickness giving a mass resolution of 2×10^{-5} g m^{-2} in the chamber. This crystal is however very sensitive to thermal gradient which limits our measurements to those of an average mass loss. After heating sequences of about 300–900 s (according to the mass loss), there must be a cooling period to recover the thermal equilibrium and determine the total mass loss by difference between the initial and the final values.

A quadrupole mass spectrometer (Hiden HAL4 EPIC300N) allows to analyze the neutral and ionized ejected species. The probe contains an internal source to ionize the neutral species and a high precision quadrupole mass filter with a mass range of 300 amu and a high sensitivity of 0.01 amu. It offers the possibility to study the neutral species by analyzing both the positive ions (due to electron impact) and the negative ions (due to electron attachment). The instrument can also analyze the negative and positive ions coming from the material by switching off the electron impact ionizer. This probe has a seven decade continuous dynamic range. The advantage of this mass spectrometer is that we can vary the emission current of the electron impact analyzer in order to know the contribution of the different species fitting with a given ratio mass per charge.

4. Experimental results

The samples which have been tested are a polycrystalline graphite (5890 grade from ''Carbone-Lorraine'') and several industrial C/C composites (called A, B, F and G) which differ from their weave, their fiber architecture (texture) or their processing routes (Table 3).

Table 3
Characteristics of the different C/C composite materials used in this study

	A	B	F	G
Fiber	Ex-PAN HR		Ex-PAN HR	
Texture	2 D	2.5 D	2.5 D	2.5 D
Weave	Twill weave		Plain weave	
Liquid consolidation	Yes	Yes	No	No
Final thermal treatment	Yes	Yes	No	Yes

To understand the influence of the different aggressions on the erosion and degradation of the material and on the composition and distribution of the ejected species, we have used two types of experimental conditions: the samples can be (i) only heated, (ii) heated and irradiated by H^+ ions. We used three temperature levels (1800, 2100 and 2400 K) in order to simulate a Sun approach. The H^+ flux is around 5×10^{16} ions m^{-2} s^{-1} with an energy of 2 keV.

4.1. The transient regime

The behavior of these C/C composites at high temperatures follows two regimes: the transient and the steady one. The transient regime corresponds to outgassing and purification processes at the beginning of the test. During this phase, the mass loss rate of graphite exhibits a temporal decrease that can be explained by a purification of the material linked to heating and outgassing in vacuum. Fig. 9 presents an example of the mass loss rate versus heating time for the composite B at the three temperature levels.

The C/C composites are processed with carbonaceous compounds like PolyAcriloNitrile polymers (PAN) that contain impurities such as oxygen, sulfur, nitrogen and halogens. Working in high vacuum, which is not the case for the processing routes, furthers the impurity release. This outgassing is due to the opening of the porous structure in the material, and to the corresponding release of the absorbed gases.

The outgassing process is characterized by the emission of impurities detected by mass spectrometry. The position of the peaks, their relative intensity and the variation of the ionization current allow to know the nature of neutral emitted species. The C/C composites emit three kind of impurities, which are minerals (Ca), nitrogenous species (N_2, NH_3, HCN) and

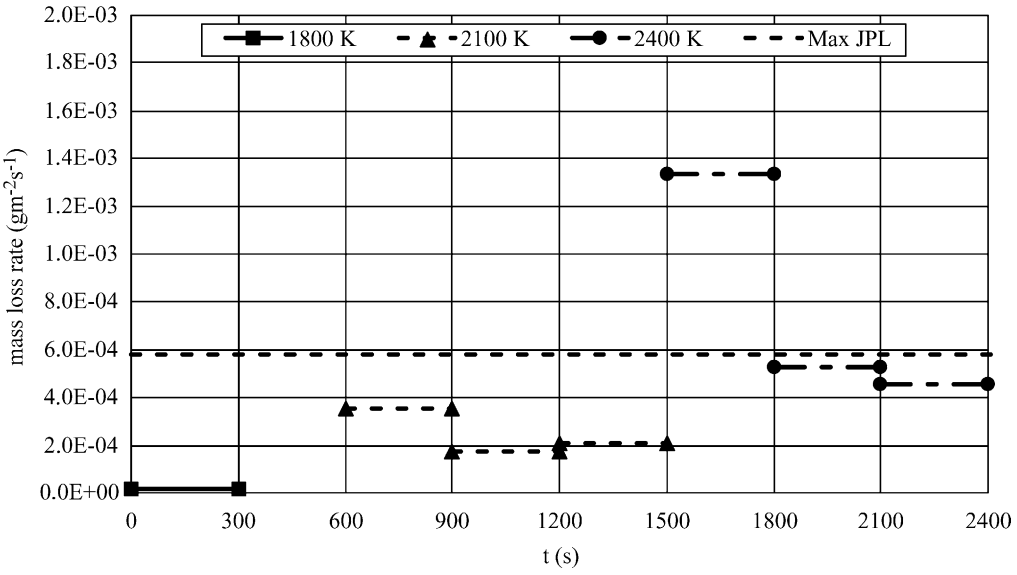

Fig. 9. Experimental average mass loss rate during the heating period of the composite B at the three temperature levels (dotted line: maximal value given by the JPL).

hydrocarbons (–CH_3, CH_4, C_2H_2, C_2H_4, C_2H_6, C_3H_3, C_3H_6, C_3H_8). For example, for the composite G, we can see some differences between the experimental two mass spectra for each regime (Fig. 10, after a heating time of 120 s and Fig. 11, after a heating time of 1200 s): the hydrocarbons and impurities peaks decrease with time, but there remains a continuum emission at the same level than the mono-atomic carbon peak due to sublimation. The outgassing is thus much longer than expected and last until around 1200 s.

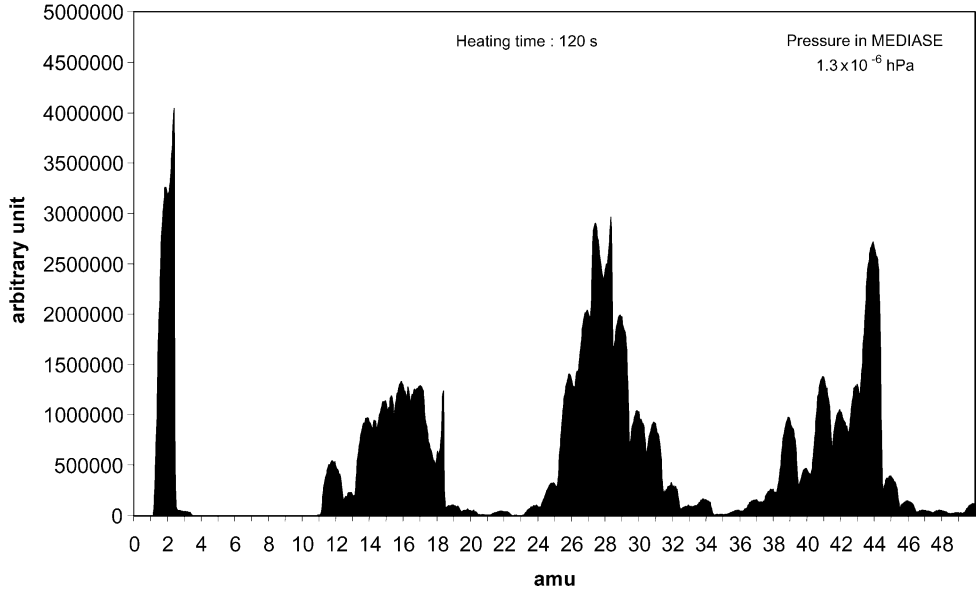

Fig. 10. Experimental mass spectrum for the composite G after 120 s heating at 2100 K without ion irradiation.

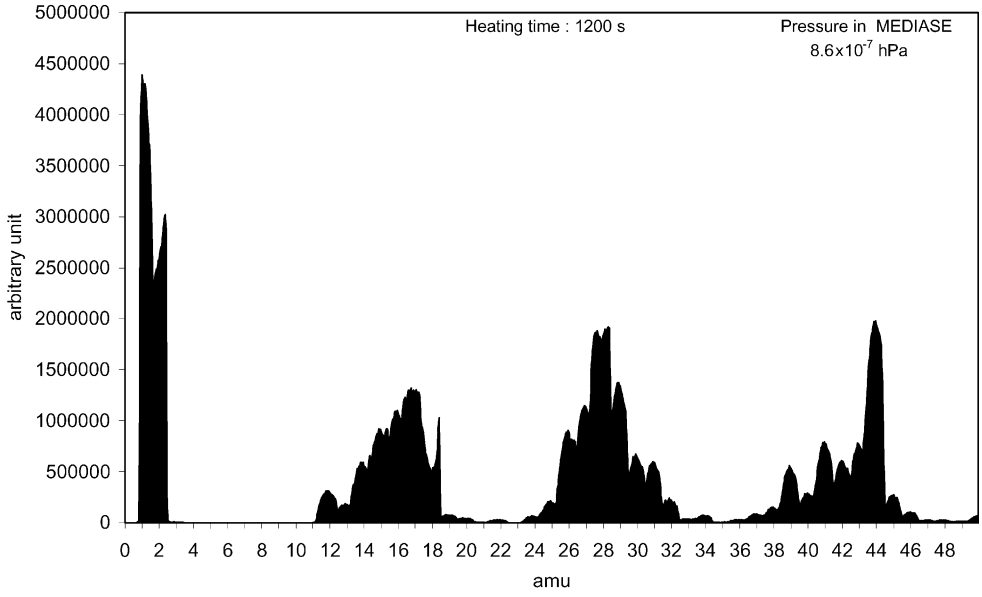

Fig. 11. Experimental mass spectrum for the composite G after 1200 s heating at 2100 K without ion irradiation.

We have also made a comparison between two composites (Fig. 12): contrary to the composite F, the composite G has been heat-treated after the processing. This treatment allows for a graphitization of the matrix and for the cleaning of the material. The initial mass loss rate for the composite F is higher than for the heat-treated composite G whereas the final mass loss rates are identical. The dominant process during the first 300 s is thus outgassing.

The fiber weave (2 D or 2.5 D) (Fig. 13) and the infiltration processes also act on the properties of the emitted species and on the mass loss rate (which are related to the graphitization).

The impurities are detectable by X-ray photoelectron spectroscopy (XPS) analysis of the condensed solid species deposited on a water-cooled gold-plated copper target located at a short distance from the sample. For all materials, Ca 2p, and N 1s photoelectron lines are

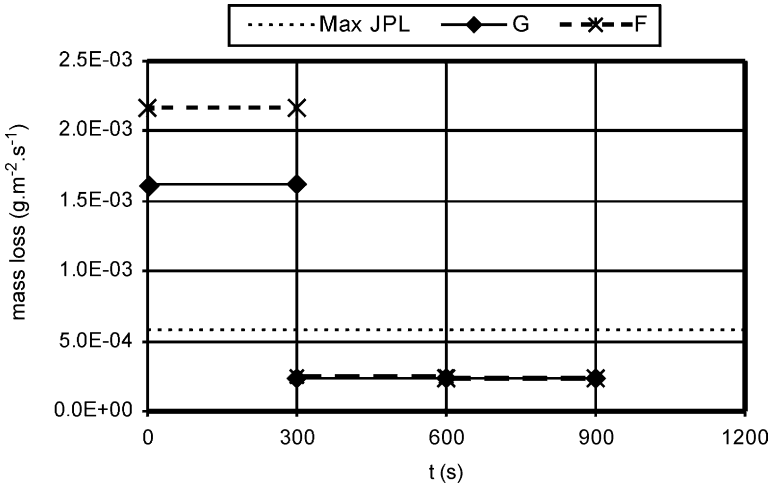

Fig. 12. Experimental average mass loss rate at 2400 K for composites F and G versus heating time (dotted line: maximal value given by JPL).

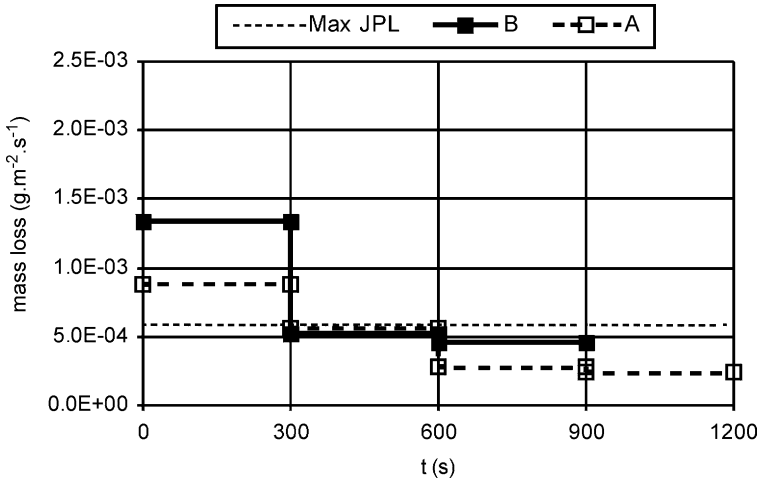

Fig. 13. Experimental average mass loss rate at 2400 K for composites A and B versus heating time (dotted line: maximal value given by JPL).

detected. A precise study of the position of these lines reveals that N is bonded to C as C–N. Moreover, the C 1s peak is also studied. The deconvolution of the C 1s peak in three peaks leads to

- the first peak corresponds to a simple bond C–O;
- the second peak is characteristic of a simple bond C–N;
- and the third one corresponds to a simple bond C–C.

By the C 1s width and the amplitude of the peak corresponding to C–N, it is possible to assert that the C–N proportion is important. Then, the C–N bond can be produced by three ways

- N is initially linked to C in the material (pores);
- C and N react in the gaseous phase during vaporization, but this last reaction is very unlikely accounting for the great mean free path of the particles;
- N reacts with the ejected carbon species.

The mass spectra have shown the importance of the peak of amu 26 and 27 corresponding to a C–N bond. Thus, the most probable hypothesis is that N is initially bonded to C in the pores of the material and that the high temperature leading to the opening of pores gives an important emission of C–N bonds.

Moreover, these impurities are released at different temperatures that depend on the material: e.g., for the polycrystalline graphite, Ca is released between 1800 and 2100 K and N between 2100 and 2400 K.

4.2. The steady regime

The mass loss rate decreases, in a way that is dependent of both time and material composition, and tends towards a limit that corresponds to the sublimation of the carbon material. This limit is experimentally lower than the detection limit at 1800 and 2100 K for the composite samples. On the contrary, in the case of polycrystalline graphite at 2400 K, the mass loss limit can be detected and is equal to $6.8 \times 10^{-4}\,\mathrm{g\,m^{-2}\,s^{-1}}$: this result is in good agreement with the theoretical estimate of $5.7 \times 10^{-4}\,\mathrm{g\,m^{-2}\,s^{-1}}$ which indicates that the main mass loss during the steady state is due to carbon sublimation and that the majority of the impurities have been released from the material.

4.2.1. Influence of the microstructure of the composite

The relative abundance of evaporated carbon species strongly depends on the composite microstructure and also differ from the theory (Table 4). Fig. 13

Table 4
Theoretical and experimental mass loss rates ($\mathrm{g\,m^{-2}\,s^{-1}}$) for the composites A and B versus temperature

T (K)	Theoretical	Experimental composite A	Experimental composite B
1800	2.6×10^{-9}	5.5×10^{-6}	4.0×10^{-5}
2100	2.8×10^{-6}	1.3×10^{-4}	2.5×10^{-4}
2400	5.7×10^{-4}	2.4×10^{-4}	4.6×10^{-4}

Table 5
Theoretical and experimental ratio C_n/C_1 for the composite B versus temperature

Composite B	C_2/C_1 (%)	C_3/C_1 (%)
Theoretical		
1800 K	4	5
2100 K	11	9
2400 K	24	15
Experimental		
1800 K	11	80
2100 K	17	39
2400 K	7	2

presents the mass loss versus time for the composites A and B which only differ by their texture, respectively 2 D and 2.5 D. In the steady state, we can notice a different behavior between these two composites. For the composite B, Table 5 shows that there is an experimental preferential emission of C_2 and C_3, contrary to the theory which assumes a preferential emission of C_1.

Fig. 14 represents the mass loss versus the initial specific area of the composite (virgin material). The mass loss increases linearly with the specific surface area.

From these two measurements, we can conclude that the morphology has a great influence on thermal sublimation of the C/C composites.

We can explain these differences by assuming that the grooves due to fibers and pores at the surface enhance the effective area. The experimental vaporization rate could be the same than the theoretical one whereas the total mass loss is much greater, due to the rugosity. The deposit thickness measured on the quartz microbalance is therefore higher than for a supposed plane surface.

4.2.2. *Influence of the temperature*

The mass loss rate increases with temperature as shown in Table 4 and Fig. 9 and differently than that expected by theory. Experimental values are hundred times greater than theoretical ones at 1800 and 2100 K. At 2400 K, the values are in the same range. Concerning the mass spectra, all the peaks increase, due to the outgassing and purification processes. The increase of the peaks corresponding to carbon species is less steep than theoretically expected. This exhibits a similar behavior that for the total mass loss rate.

The surface defects appear to be the dominant process of the composite vaporization. The gradual

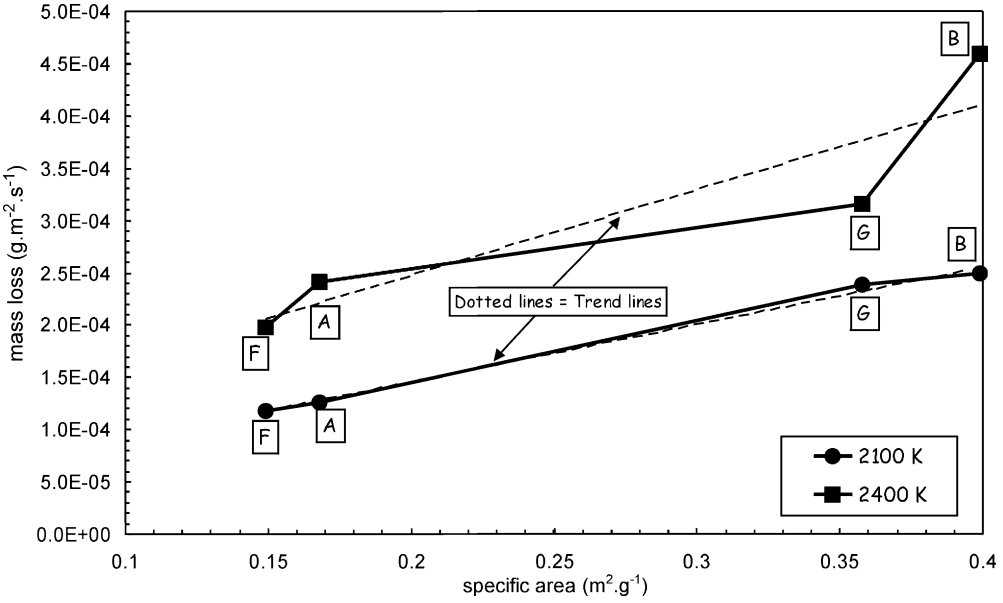

Fig. 14. Relation between the experimental mass loss rate of all the composites and their specific area at 2100 and 2400 K (dotted lines = trend lines).

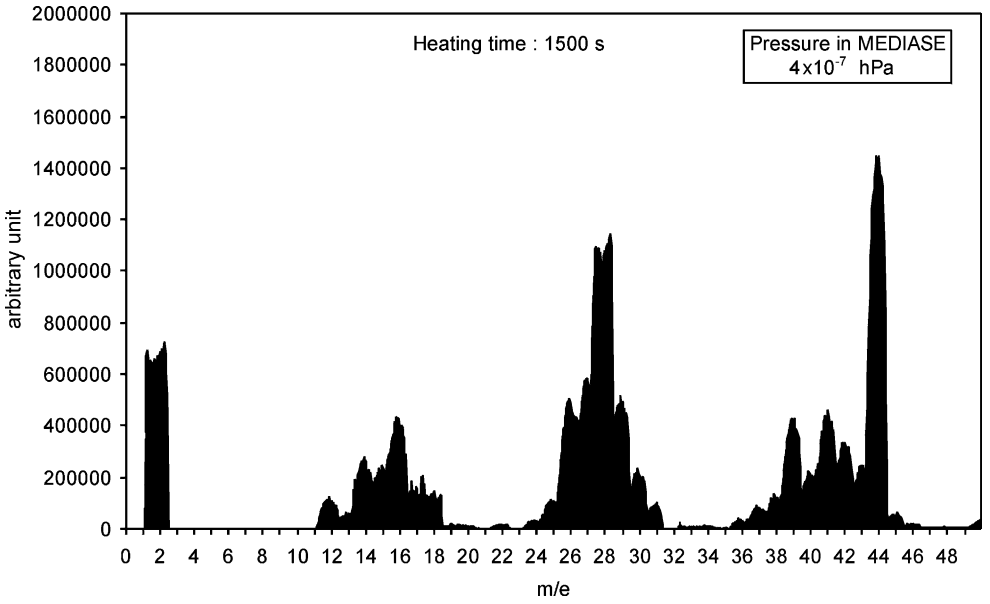

Fig. 15. Experimental mass spectrum for the composite B at 2100 K without proton irradiation.

opening of closed pores will also further this effect, which will cause serious problems for the using of C/C composites as thermal-protection system if an outgassing at around 2400 K is not performed during the processing route of the material.

4.2.3. Influence of ion irradiation

In our experimental conditions, the ion irradiation is responsible of two sputtering processes: physical and chemical erosions.

By comparing Figs. 15 and 16 of the experimental mass spectra for the composite B obtained after 1500 s at 2100 K respectively without (Fig. 15) and with proton irradiation (Fig. 16), an emission of carbon atoms due to ion irradiation is detected. The intensity ratio of the peak of amu 12 with and without irradiation, at 1800 and 2100 K are reported in Table 6 for the composites B and G. These intensities were obtained for an ionization energy of 30 eV in order to minimize the contribution of hydrocarbons on this peak of amu 12. This ratio decreases when the temperature increases, i.e. the contribution of the physical sputtering with regards to the thermal sublimation is less important when the temperature increases as theoretically predicted.

Table 6
Intensity ratio of peak of amu 12 with and without ion irradiation for the composites B and G

	Composite B	Composite G
1800 K	4.0	4.8
2100 K	1.1	2.0

Fig. 17 shows the ratio of carbon fluxes with ion irradiation. The lines are theoretical ratios taking into account RES or not. The points are experimental values obtained for the composites B and G: we can notice that the experimental values fit well with the theory without RES, which means that RES has a small influence on the total sputtering yield. This can be explained by the fact that the thermal emission of interstitial atoms produced by collisional processes is negligible comparing to atomic carbon flux due to physical sputtering.

The chemical sputtering due to ion irradiation is characterized by the emission of CH_3, acetylene and propene. These species are characterized by the increase of three groups with amu respectively equal to (15), (24, 25, 26) and (39, 40, 41, 42) (Figs. 15 and 16).

The peak of amu 15 is increased by a factor 3 with ion irradiation.

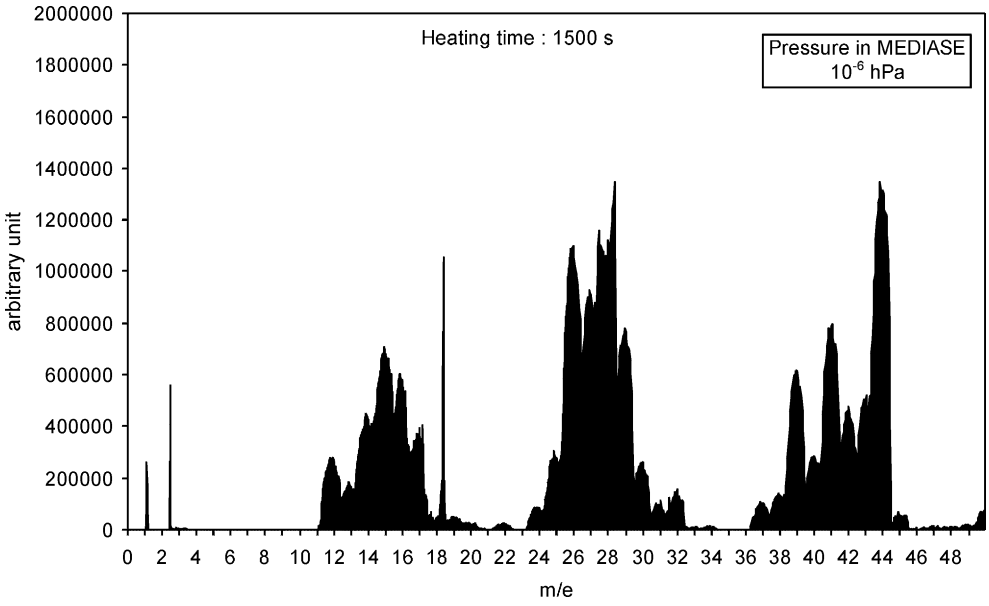

Fig. 16. Experimental mass spectrum for the composite B at 2100 K irradiated by protons (H^+, 2 keV, 5×10^{16} ions m^{-2} s^{-1}, 45°).

For the group of amu 24–26, their relative proportions according to the mass 26 are respectively, at 2100 K for the composite B, 8, 26 and 100 and for the composite G, 7, 23 and 100. The theoretical proportions for these masses for acetylene are equal to 6, 20 and 100. Thus, the increase of these peaks is characteristic of an emission of acetylene under ion irradiation.

For the group of amu 39–42, their relative proportions according to the mass 41 are respectively, at 2100 K for the composite B, 78, 36, 100 and 61 and for the composite G, 79, 43, 100 and 75. The theoretical proportions for these masses for propene are equal to 77, 29, 100 and 66. Thus, the intensities of these peaks are characteristic of an emission of propene under ion irradiation. We have to notice that the maximum

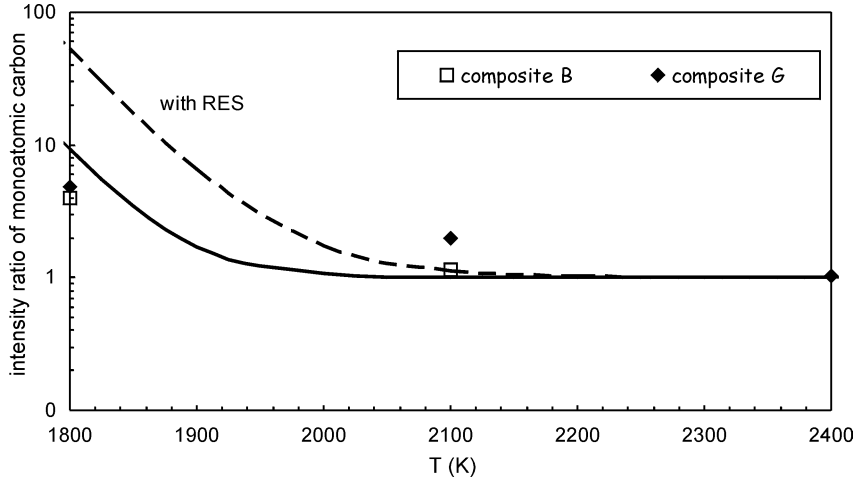

Fig. 17. Intensity ratio of mono-atomic carbon emission due to physical sputtering, thermal sublimation with and without RES (respectively, dotted and continuous lines) versus temperature with the experimental points obtained for the composites B and G.

intensity for the peak of propene is not at amu 42, but at amu 41 corresponding to the ionized species $C_3H_5^+$.

Moreover, the fluxes of these species depend on the composite: e.g., the composite G, in the same experimental conditions emits 30% in acetylene and 46% in propene more than the composite B. The analyses of the ionization curves for the peaks of amu 12 and 26 and the calculation of the fluxes for an ionization energy of 30 eV show that the fluxes of acetylene and propene are 30 times greater than the flux of mono-atomic carbon. It seems that there is no relationship between the specific area and these fluences, because the composite G emits more hydrocarbons than B in spite of its lower specific area.

The emission of propene has not been theoretically explained but this emission must come from the reaction between H_2 and carbon atoms.

We have also observed that the ion irradiation does not lead to a significant formation of methane (peak of amu 16) but of CH_3 (peak of amu 15), and also that no molecular hydrogen (peak of amu 2) is emitted contrary to the theory. However, the disappearance of the H_2 emission is in good agreement with literature [26].

As a conclusion, the three main sputtering processes in our experimental temperature range are the outgassing, the thermal sublimation and the chemical sputtering.

4.2.4. The ejected ionized species

The mass spectrometer allows to analyze the ionized ejected species. The only positively charged particles emitted by the carbon material correspond to H^+ ions (amu 1). These ions come from the backscattering of the incident protons at the surface of the sample.

The ion irradiation of the composites gives rise to the emission of H^- ions for all composites and to the emission of C^- and C_2^- for the composite F which has not been heat-treated during its elaboration. This could be due to a charge transfer between the incident ions and the carbon target and to a change of the electronic configuration of graphite.

5. Conclusion

Several conclusions can be drawn from these experimental results concerning the influence of the C/C composite structure on the behavior at high temperatures under ion irradiation.

First of all, the composite microstructure has an important influence on the mass loss rate. The fiber weave of the material acts on the matrix structure (degree of graphitization, defects concentration) and on the surface morphology. An important rugosity enlarges significantly the effective area of the treated surface leading to a steep increase of the total mass loss rate of the sample. Moreover, the opening of the pores enhances the initial rugosity and furthers the mass loss. Comparing the theoretical and experimental mass spectra and the C_n/C_1 ratio, we have noticed that the pulling-out of the carbon species strongly depends on surface morphology and that the materials are submitted to an outgassing which overcomes the sublimation rate during the first 300 s of the tests. This outgassing is mainly due to the release of some impurities (N_2, Ca and hydrocarbons) of the material at their temperature of vaporization.

During the steady regime, for temperatures above 2400 K, the thermal sublimation overcomes the other sputtering processes (chemical, physical and RES). At 1800 and 2100 K, the thermal sublimation is characterized by the emission of mono-atomic carbon. But, between 2100 and 2400 K, the experimental fluxes of C_2 and C_3 species increase with temperature and at 2400 K, they are more important than the flux of mono-atomic carbon.

The chemical sputtering is, however, responsible of an important emission of acetylene and propene. At 2100 K, the fluxes of acetylene and propene are higher than the carbon fluxes due to thermal sublimation.

The RES and the physical sputtering have only a weak influence on the total sputtering yield contrary to what was expected by modeling, but could damage the surface and disturb the material structure.

So, the three main sputtering processes in our experimental temperature range are the outgassing, the thermal sublimation and the chemical sputtering.

Finally, the majority of ionized ejected species are H^+ ions mainly due to the backscattering of ions at the material surface and H^- due to a charge transfer.

The perspective under consideration, to study more accurately the sputtering processes will be to perform a calibration using known gas quantities in order to

calculate the real fluxes obtained by mass spectrometry to reach the sputtering yield of the carbon materials, as already proposed by Dobrozemsky [27,28].

Another important study remains to be done on the post-treatment characterization of the C/C composites. Several techniques will be used to study the induced damages and the evolution of the microstructure and surface morphology. Raman spectroscopy will allow us to study the microstructure and the defect-induced features at the surface of the composites, and for X-ray diffraction the same parameters in the bulk. Raman spectroscopy will also probe the evolution of the chemical bonding (sp^2 to sp^3). A SEM characterization will show us the possible fracture induced at the surface and a STM observation the evolution of morphology in the atomic scale. This last study is very important since the rugosity has a great influence on the thermo-radiative properties and thus on the temperature of the material.

Acknowledgements

The authors want to thank the 1000 kW IMP-CNRS Odeillo team, J. Bouyssou and J. Rouzaud from CESR-CNRS for their technical assistance in mass spectrometry and instrumental design, CNES, EADS-LV and SNECMA-Moteurs for the financial support of this work and for the composite material supply.

References

[1] J.M. Millard, R.N. Miyake, R.B. Dirling, A. Rolfo, C. Royere, Starprobe thermal shield evolution, in: Proceedings of the International Symposium on Environmental and Thermal Systems for Space Vehicles, Toulouse, France, October 4–7, 1983, pp. 531–560.

[2] O. Vaisberg, B. Tsurutani (Eds.), in: Proceedings of the First US–Russian Scientific Workshop on FIRE Environment, Space Research Institute, Moscow, June 5–7, 1995.

[3] R. Behrisch, et al., Sputtering by Ion Bombardment, Vol. I, Topics in Applied Physics, No. 47, Springer, Berlin, 1981.

[4] R. Behrisch, et al., Sputtering by Ion Bombardment, Vol. II, Topics in Applied Physics, No. 52, Springer, Berlin, 1983.

[5] W. Eckstein, Computer Simulation of Ion–solid Interactions, Springer Series in Materials Science, Vol. 10, Springer, Berlin, 1991.

[6] W. Möller, W. Eckstein, J.P. Biersack, TRIDYN — binary collision simulation of atomic collisions and dynamic composition changes in solids, Comput. Phys. Commun. 51 (1988) 355–368.

[7] J. Roth, E. Vietzke, A.A. Haasz, Erosion of graphite due to particle impact, Atomic Plasma–Material Interact, Data For Fusion (Suppl. to Nucl. Fusion) 1 (1991) 63–78.

[8] V. Philipps, Plasma wall interaction and its control by wall conditioning, Trans. Fusion Technol. 33 (1998) 261–272.

[9] A.A. Haasz, P. Franzen, J.W. Davis, S. Chiu, C.S. Pitcher, Two-region model for hydrogen trapping in and release from graphite, J. Appl. Phys. 77 (1995) 66–85.

[10] J. Roth, C. Garcia-Rosales, Analytic description of the chemical erosion of graphite by hydrogen ions, Nucl. Fusion 36 (12) (1996) 1647–1659.

[11] M. Balooch, D.R. Olander, Reactions of modulated molecular beam with pyrolytic graphite. III. Hydrogen, J. Chem. Phys. 63 (11) (1975) 4772–4786.

[12] J. Roth, J. Bohdansky, K.L. Wilson, Erosion of carbon due to bombardment with energetic ions at temperatures up to 2000 K, J. Nucl. Mater. 111/112 (1982) 775–780.

[13] J. Roth, W. Möller, Mechanism of enhanced sputtering of carbon at temperatures above 1200°C, Nucl. Instr. Meth. Phys. Res. B 7/8 (1985) 788–792.

[14] V. Philipps, E. Vietzke, H. Trinkaus, Radiation enhanced sublimation of carbon and carbon related materials, J. Nucl. Mater. 179–181 (1991) 25–33.

[15] Y. Ueda, K. Shiota, Y. Kitamura, Y. Ohtsuka, M. Isobe, M. Nishikawa, Detailed study of radiation enhanced sublimation of graphite under high flux beam irradiation, Fusion Eng. Des. 41 (1998) 55–61.

[16] M. Küstner, W. Eckstein, V. Dose, J. Roth, The influence of surface roughness on the angular dependence of the sputter yield, Nucl. Instr. Meth. Phys. Res. B 145 (1998) 320–331.

[17] M. Nishikawa, High flux dependence of erosion and retention in beam experiments and its significance to fusion systems, Fusion Eng. Des. 41 (1998) 47–53.

[18] Y. Yamamura, Computer studies of reemission and depth profiles for helium on molybdenum, Nucl. Instr. Meth. Phys. Res. B 28 (1987) 17–26.

[19] T. Kenmotsu, T. Kawamura, L. Zhijie, T. Ono, Y. Yamamura, Simulation studies on sputtering and reflection from compound materials at elevated temperatures, J. Nucl. Mater. 266–269 (1999) 557–560.

[20] M. Wittmann, J. Küppers, A model of hydrogen impact induced chemical erosion of carbon based on elementary reaction steps, J. Nucl. Mater. 227 (1996) 186–194.

[21] J. Roth, Chemical erosion of carbon based materials in fusion devices, J. Nucl. Mater. 266–269 (1999) 51–57.

[22] W. Eckstein, C. Garcia-Rosales, J. Roth, W. Ottenberger, Sputtering Data, Internal Report (Max-Planck-Institut für Plasmaphysik) IPP 9/82, February 1993.

[23] J.P. Biersack, L.G. Haggmark, A Monte Carlo computer program for the transport ions in amorphous targets, Nucl. Instr. Meth. B 174 (1980) 257–269.

[24] J. Lindhard, M. Scharff, Energy dissipation by ions in the keV region, Phys. Rev. 124 (1961) 128–130.

[25] M.W. Chase, J.R. Davies, J.R. Downey, D.J. Frurip, R.A. McDonald, A.N. Syverud, JANAF Thermodynamical Tables, 3rd Edition, J. Phys. Ref. Data 14 (1985).
[26] P. Franzen, E. Vietzke, Atomic release of hydrogen from pure and boronized graphites, J. Vac. Sci. Technol. A 12 (3) (1994) 820–825.
[27] R. Dobrozemsky, Calibration of vacuum systems by gas quantities, Vacuum 41 (7–9) (1990) 2109–2111.
[28] R. Dobrozemsky, G.W. Schwarzinger, Mass spectrometry of fusion-plasma gases, J. Vac. Sci. Technol. A 10 (4) (1992) 2661–2664.